RESEARCH ARTICLE

Key Points:
- Two distinct types of nighttime MSTIDs have been identified and classified in relation to their morphology and wave characteristics
- The anisotropy observed in the dark band and periodic MSTID propagation direction can be explained by different physical mechanisms
- We have shown that the gravity waves resulting in MSTIDs can propagate from the troposphere without reaching the critical level

Supporting Information:
- Supporting Information S1
- Movie S1
- Movie S2
- Movie S3

Correspondence to:
C. A. O. B. Figueiredo,
cosme.figueiredo@inpe.br;
anagetinga@gmail.com

Investigation of Nighttime MSTIDS Observed by Optical Thermosphere Imagers at Low Latitudes: Morphology, Propagation Direction, and Wind Filtering

C. A. O. B. Figueiredo[1] ID, H. Takahashi[1] ID, C. M. Wrasse[1] ID, Y. Otsuka[2] ID, K. Shiokawa[2] ID, and D. Barros[1] ID

[1]Instituto Nacional de Pesquisas Espaciais, São José dos Campos, Brazil, [2]Institute for Space-Earth Environmental Research, Nagoya University, Nagoya, Japan

Abstract Different types of medium-scale traveling ionospheric disturbances (MSTIDs) have been observed at Cachoeira Paulista (22.4°S; 45.0°W), Brazil, from June 2013 to December 2015, using airglow OI 630.0-nm images. During the period, 58 MSTIDs were identified and classified as follows: dark band MSTIDs (around 10 events) and periodic MSTIDs (48 events). Dark band MSTIDs present phase velocity between 50 and 200 m/s and propagation direction to northwestward. On the other hand, periodic MSTIDs have phase velocity of 50 to 200 m/s, horizontal wavelengths from 80 to 160 km, periods ranging between 5 and 45 min, and propagation directions are mainly north-northeastward. The wave parameters indicate that periodic MSTIDs have different characteristics when compared to dark band MSTIDs, suggesting that periodic MSTIDs are not generated through the well-known Perkins and *E-F* coupling instability. In addition to it, the present study indicates that the spectral characteristics found in Brazil are different from other regions such as Japan and Indonesia. Therefore, we intend to do the statistics of the wave parameters (wavelength, phase velocity, period, propagation direction, and time occurrence) and investigate the generation mechanisms of periodic MSTIDs at low to middle latitude for the first time. Furthermore, the anisotropy observed in periodic MSTID propagation direction can be explained by different mechanisms.

1. Introduction

Traveling ionospheric disturbances (TIDs) are perturbations in the ionospheric plasma with wavelengths of range of hundreds to thousands kilometers and speed of the order of hundreds to thousands meters per second (Hunsucker, 1982; Kelley, 2011). The TIDs are divided into three types: small scale (e.g., Alimov et al., 2008), medium scale (MSTID; e.g., Figueiredo et al., 2018; Otsuka et al., 2013), and large scale (e.g., Figueiredo, Wrasse, et al., 2017). It is important to study TIDs at low latitudes because they trigger equatorial plasma bubbles (e.g., Takahashi et al., 2018).

MSTIDs have been, first, studied by Hines (1960), and since then, many theoretical studies have been published, such as Francis (1974), Yokoyama et al. (2004), Yokoyama et al. (2009), and Yokoyama and Hysell (2010). Furthermore, MSTIDs have been observed by several techniques, such as ionosondes (e.g., Amorim et al., 2011; Bowman, 1985, 1989; Munro, 1948), satellites (e.g., Forbes et al., 2016), airglow images (e.g., Candido et al., 2008; Garcia et al., 2000; Mendillo et al., 1997; Paulino et al., 2016; Shiokawa, Ihara, et al., 2003), incoherent scatter radar (e.g., Medvedev et al., 2017), and Global Navigation Satellite System (e.g., Otsuka et al.. 2013).

Most of nighttime MSTIDs have propagation direction to northwestward (southwestward) in Southern (Northern) Hemisphere. For this reason, Perkins instability is considered to be responsible for the generation of nighttime MSTIDs. However, the result obtained by Cosgrove and Tsunoda (2003, 2004) and Cosgrove et al. (2004) showed that the growth rate of Perkins instability is very small and does not match observations. In this way, it was necessary to look for other mechanisms that allow Perkins instability to develop faster, for example, polarization electrical field (Behnke, 1979; Fukao et al., 1991; Kelley & Fukao, 1991; Kelley et al., 2000; Makela & Kelley, 2003; Otsuka et al., 2004, 2009; Saito et al., 2008; Shiokawa, Otsuka, et al., 2003; Shiokawa et al., 2005) and coupling between *E* and *F* regions (Cosgrove & Tsunoda, 2004; Cosgrove et al., 2004; Haldoupis et al., 1996; Kelley et al., 2003; Otsuka et al., 2007; Tsunoda, 1998; Tsunoda & Cosgrove, 2001; Yokoyama & Hysell, 2010; Yokoyama et al., 2009, 2004).

The first reports of nighttime MSTID observations using *All-Sky* imagers in South America have been made by Sobral et al. (2001), at Cachoeira Paulista, Brazil, and Martinis et al. (2006), at El Leoncito (31.8°S, 69.3°W), Argentina. Pimenta, Amorim, and Candido (2008) and Pimenta, Kelley, et al. (2008) studied dark band MSTIDs at Cachoeira Paulista using a database of 5 years of observations. Pimenta, Kelley, et al. (2008) verified that dark band MSTIDs occur in winter and are more frequent in the period of low solar activity and ascending phase, its propagation directions are distributed between 280° and 320° (west-northwest) and propagation velocity between 50 and 200 m/s. Candido et al. (2008) performed a similar study to that of Pimenta, Kelley, et al. (2008), in which the authors attribute Perkins instability as the main mechanism to explain propagation direction and origin of dark band MSTIDs. Recently, Amorim et al. (2011) also used ionosonde data to obtain values of h'F and foF2, which also present an appearance of spread *F* associated with dark band MSTIDs. Duly et al. (2013) observed MSTIDs in the inter-American observatory Cerro Tololo (30.17°S, 70.81°W), Chile. Observations carried out by Stefanello et al. (2015) presented two nighttime MSTIDs at conjugated points, over São Martinho da Serra (29.4°S, 53.8°W), Brazil, and Ramey (18.5°N, 67.1°W), Puerto Rico. The MSTID was observed by several types of equipment such as ionosonde, GPS receivers, and All-Sky imager. The authors suggested that the South Atlantic magnetic anomaly contributed to the linear growth of Perkins instability and amplification of the polarization electric field; consequently, wave structures were mapped for their respective magnetic conjugate.

Paulino et al. (2016) carried out a study using 10 years (September 2000 to November 2010) of airglow images from equatorial to low-latitude region, São João do Cariri (7.4°S, 36.5°W). The authors observed that MSTIDs present periodic structures, different from the dark band MSTIDs studied by Pimenta, Amorim, & Candido (2008), Pimenta, Kelley, et al. (2008), Candido et al. (2008), and Amorim et al. (2011). Periodic MSTIDs have a horizontal wavelength between 100 and 200 km, period ranging from 10 to 35 min, and phase velocity from 10 to 180 m/s. The authors also calculated the propagation directions and verified that MSTIDs propagate to north-northeast and southeast with higher occurrence during high solar activity period and winter months (June to August). Paulino et al. (2016) suggested that the upward gravity waves from troposphere are the source of periodic MSTIDs. Paulino et al. (2018) calculated the intrinsic parameters of periodic MSTIDs in the equatorial region of Brazil between 2012 and 2014 using neutral winds obtained by Fabry-Perot interferometers. The authors noticed that most of the observed MSTIDs had intrinsic periods lower than the observed periods, that is, the intrinsic phase velocity was faster. Therefore, these waves can propagate more easily in the thermosphere/ionosphere, because gravity waves can skip critical levels and turning (Vadas, 2007). However, statistical study, source location, and the effects of the thermospheric winds in the propagation direction of these periodic MSTIDs from low to middle latitudes at Cachoeira Paulista (22.7°S, 45.0°W) have not been carried out yet.

The main goal of the present paper is to distinguish, for the first time, between dark band and periodic MSTIDs in terms of morphology and wave parameters (wavelength, phase velocity, period, propagation direction, and time occurrence), observed at low to middle latitudes.

2. Instrumentation and Methodology

All-Sky imager installed at Cachoeira Paulista was used to observe nighttime MSTIDs between June 2013 and December 2015. The oxygen red line emission, OI 630.0 nm, was used to observe thermosphere nighttime MSTIDs.

The All-Sky imager is composed by a fisheye lens, a telecentric lens system, a filter wheel on which interference filters are housed, a lens set to reconstruct the image, and a Charge Coupled Device camera. The Charge Coupled Device camera used in this study consists of a 1.77-cm^2 sensor, air cooled by a Peltier system, and presents high quantum efficiency of 95%. The images are obtained from the 110-s time integration of the OI 630.0 nm emission. The OI 630.0-nm filter used in this study has the following characteristics: filter diameter = 3″, peak wavelength = 630.550 nm, and bandwidth = 2.00 nm. OI 630.0 nm images are affected by contamination from OH (9, 3) Meinel band emission. This happens because a few lines of the OH (9, 3) P branch are located in the wavelength region of the band-pass filter. When such contamination occurs, the waves occurring in OH layer heights will be also observed in the OI 630-nm images. Therefore, measuring OI 630.0 nm and OH near infrared emissions separately, we checked whether each event has OH emission
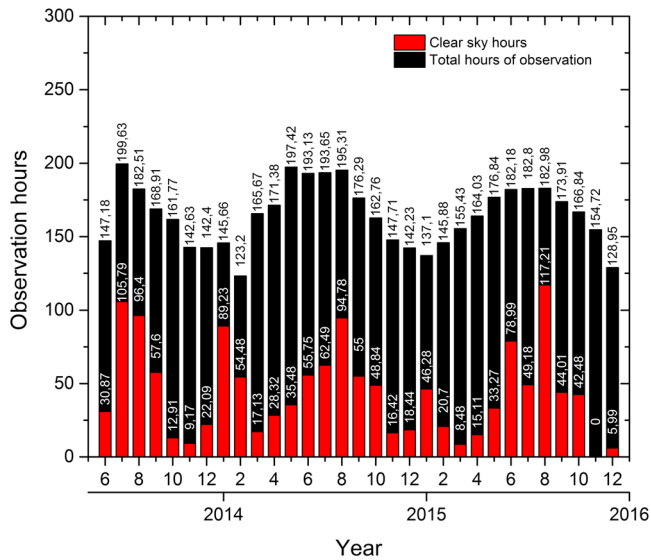
Figure 1. Number of hours per month in which airglow observations were carried out (black bars), as well as the hours of observation with clear sky (red bars). The observed period is between June 2013 and December 2015.

contamination and removed it for analysis. The methodology used is to compare, in the same time span, OH and OI 630.0 nm by watching videos and check if there is any contamination, that is, if the waves are equal.

Figure 1 shows the total number of hours observed (black bars) and the number of hours with clear sky (red bars). In this work, 5,171 hr of observation was obtained between June 2013 and December 2016 and only ~ 27% with a clear sky. During winter months, it is observed the largest amount of clear skies, whereas for summer months, cloud cover increases considerably. The MSTIDs observed in this study correspond to 5.2% (72.0 hr) of the total number of hours of observation with clear sky.

Before analyzing the images to extract the wave parameters of nighttime MSTIDs, it is necessary to preprocess them. The main stages of image preprocessing can be listed as follows: align the image with geographic north, remove the stars, and unwarping the image; each image in the data set was spatially filtered with a second-order high-pass Butterworth filter, with cutoff frequencies at 30 km for projections onto $1,024 \times 1,024$ km (resolution of 2 km/pixel). This high-pass filter is used to eliminate low frequencies due to background noise contamination (Bageston et al., 2011). In addition, this filter makes the image to emphasize MSTIDs oscillation. Then a cross-spectral analysis was performed applying a standard two-dimensional fast Fourier transform. The main MSTID parameters can be determined, such as the phase velocity, horizontal wavelength, period, and propagation direction. The details of each step can be found in Medeiros et al. (2003), Wrasse et al. (2007), and Paulino et al. (2016).

3. Results

The MSTIDs observed at Cachoeira Paulista were classified into two types: dark bands and periodic waves. Dark bands MSTIDs have been extensively studied by Pimenta, Amorim, and Candido (2008), Candido et al. (2008), and Amorim et al. (2011). On the other hand, periodic MSTIDs have been characterized (wavelength, period, velocity, propagation direction, and seasonality) only in Brazilian equatorial region by Paulino et al. (2016 and 2018). The 1-year interval was divided into four seasons: southern summer (December–February), southern autumn (March–May), southern winter (June–August), and southern spring (September–November).

3.1. Dark Band MSTIDs

The criteria for identifying dark band MSTIDs are a well-defined wavefront followed by a dark region; dark band MSTIDs cover almost the entire image with phase front extending more than 1,000 km; the phase front propagates in only one direction; dark band MSTIDs could be observed for at least 30 min.

We observed 10 dark band MSTIDs. Figure 2 shows a dark band MSTID propagating northwestward, indicated by the white arrows, between 02:00 and 03:00 UT (22:00 and 24:00 LT) on the night of 5 July 2013. Top of Figure 2 refers to the geographical north, and the right-hand side of the image refers to the geographical east. The projection of the images is $1,024 \times 1,024$ km (resolution of 2 km/pixel). The Milky Way is visible in the center of the image. An animation of Figure 2 is available through the supporting information related to this paper (see Movie S1).

Figure 3 shows the monthly occurrence rate of dark band MSTIDs. The monthly occurrence rate is defined as the ratio of the number of hours in which dark band MSTIDs are observed at a given time interval, for example, between 01 and 02 UT, and the number of hours of observation with clear sky for each month. The predominance of dark band MSTIDs occurrence is from June to October, between 22:00 and 03:00 LT, in southern winter and early southern spring. Similar results were observed by Pimenta, Amorim, and Candido (2008) and Candido et al. (2008).

Figure 4 shows the propagation directions of dark band MSTIDs as a function of velocity. The distribution of the propagation direction was anisotropic, with west-northwest propagation. The velocity of dark band MSTIDs obtained in this work range between 50 and 200 m/s.
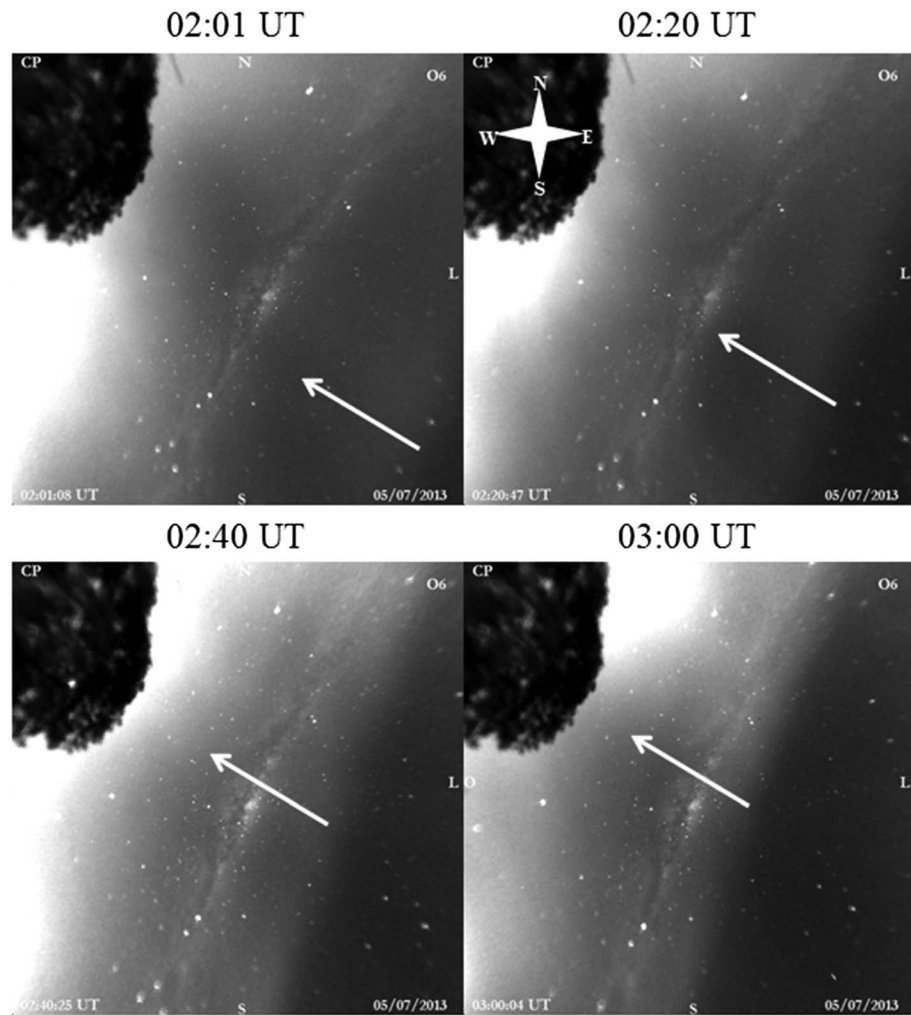
Figure 2. Unwarped images sequence, where it is possible to visualize a dark band medium-scale traveling ionospheric disturbance propagating northwestward, indicated by white arrows, on the night of 5 July 2013, between 02:00 and 03:00 UT (23:00 and 24:00 LT).
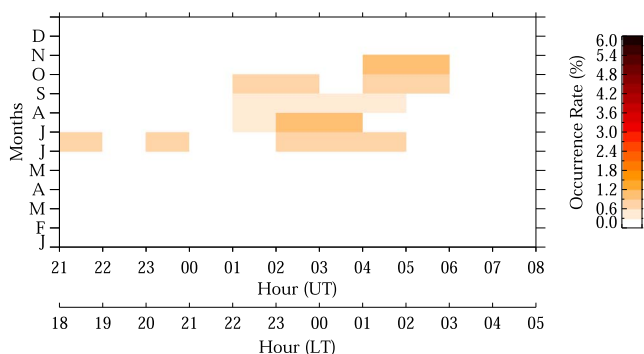
Figure 3. Occurrence rate of dark band medium-scale traveling ionospheric disturbances as a function of time. The letters denote the months of the year.

3.2. Periodic MSTIDs

Paulino et al. (2016) characterized nighttime periodic MSTIDs in the Brazilian equatorial region. However, in low to middle latitudes (south-southeast of Brazil) these waves had not been characterized yet.

The criteria used in the present work for identification of periodic MSTIDs in the OI 630.0 nm images are as follows: presenting wave structure, that is, more than two wavefronts, propagating for at least 30 min, and phase front shorter than 1,000 km.

Figure 5a shows a periodic MSTID propagating to north-northeast, indicated by the white arrows, over Cachoeira Paulista on 2 August 2013, between 22:31 and 23:03 UT. The structure in the right-hand side of MSTID is the Milky Way. Figure 5b shows images of the OH emissions, in the same time span of Figure 5a. Comparing the images, we can see that the MSTID in the OI 630 nm does not suffer contamination of the OH emission. An animation of Figure 5a is available through the supporting information related to this paper (see Movie S2). In addition, an animation of
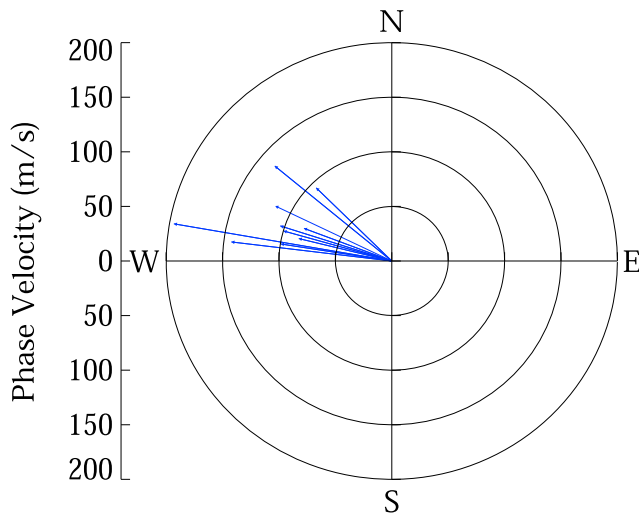
Figure 4. Vector diagram showing propagation direction of dark band medium-scale traveling ionospheric disturbances as a function of azimuth and phase velocity observed between June 2013 and December 2015.

OH images, Figure 5b, in the same time span of Figure 5a, is available through the supporting information related to this paper (see Movie S3).

In this work, 48 periodic MSTIDs were observed during the period from June 2013 to December 2015.

Figure 6 shows the monthly occurrence of periodic MSTIDs as a function of time. The occurrence rate is defined as the ratio of the number of hours in which periodic MSTIDs are observed at a given time interval, for example, between 01 and 02 UT, and the number of hours of observation with clear sky for each month.

Periodic MSTIDs are observed more in the early evening, between 21:00 and 3:00 UT (18:00 and 00:00 LT), from May to September. Few cases are observed out of this range. In November, it is observed that the occurrence of periodic MSTIDs is very high, but this is due to the few hours of observation with clear sky.

Figure 7a shows the horizontal wavelength distribution as a function of the occurrence of periodic MSTIDs. Most of the waves have horizontal wavelengths between 90 and 130 km, with an average value of 111 km and a standard deviation of 15 km. Using airglow images, it is possible to observe horizontal wavelengths in the OI 630.0-nm emission of up to ~1,500 km.

Distribution of the observed periods of periodic MSTIDs is presented in Figure 7b. Periodic MSTIDs present an observed period between 10 and 25 min, with an average of 21 min and its respective standard deviation of 15 min. Intrinsic periods of Brünt Väissälä at around 250 km of altitude (OI 630.0-nm emission layer) are around 8–9 min Vadas, 2007).

Figure 7c shows the distribution of the horizontal phase velocity of the periodic MSTIDs. It is observed that most periodic MSTIDs have phase velocities ranging from 80 to 140 m/s and mean values of 103 ± 33 m/s.

Figure 8 shows propagation directions of periodic MSTIDs as a function of the horizontal phase velocity for all 48 wave events. The distribution of wave propagation is not isotropic but rather anisotropic. Most of the waves propagate to north and northeast directions. When these results are compared with the propagation direction of dark band MSTIDs, we can notice that they are different; thus, in the discussions we will discuss if dark band and periodic MSTIDs are originated by the same physical processes.

Reviewing the literature, we can identify and classify two distinct types of nighttime MSTIDs in relation to their morphology and wave characteristics: dark bands (Amorim et al., 2011; Candido et al., 2008; Duly et al., 2013; Garcia et al., 2000; Kelley, 2011; Kotake et al., 2006; Martinis et al., 2006, 2010; Otsuka et al., 2013; Pimenta, Amorim, & Candido, 2008; Pimenta, Kelley, et al., 2008; Shiokawa, Ihara, et al., 2003; Shiokawa, Otsuka, et al., 2003) and periodic MSTIDs (Fukushima et al., 2012; Paulino et al., 2016, 2018; Sau et al., 2018; Shiokawa et al., 2006; Sobral et al., 2001). Table 1 summarizes the characteristics of the two types of nighttime MSTIDs. Based on the characteristics of nighttime MSTIDs, we would suggest to the scientific community to have different nomenclatures for the phenomena: those that are generated under the condition of Perkins instability and have electrodynamic characteristics are called Perkins MSTIDs, and those with gravity waves' characteristics are called gravity waves MSTIDs.

4. Discussions

The present study focuses on the MSTIDs observed in low to middle latitudes (15–35°S) and tries to distinguish MSTIDs triggered by Perkins instability and by gravity waves propagation.

4.1. Dark Band MSTIDs

The predominance of dark band MSTIDs occurrence is from June to October, between 22:00 and 03:00 LT, in the southern winter and early southern spring. Similar results were observed by Pimenta, Amorim, and Candido (2008) and Candido et al. (2008). Park et al. (2015) shows Midlatitude Magnetic Fluctuations
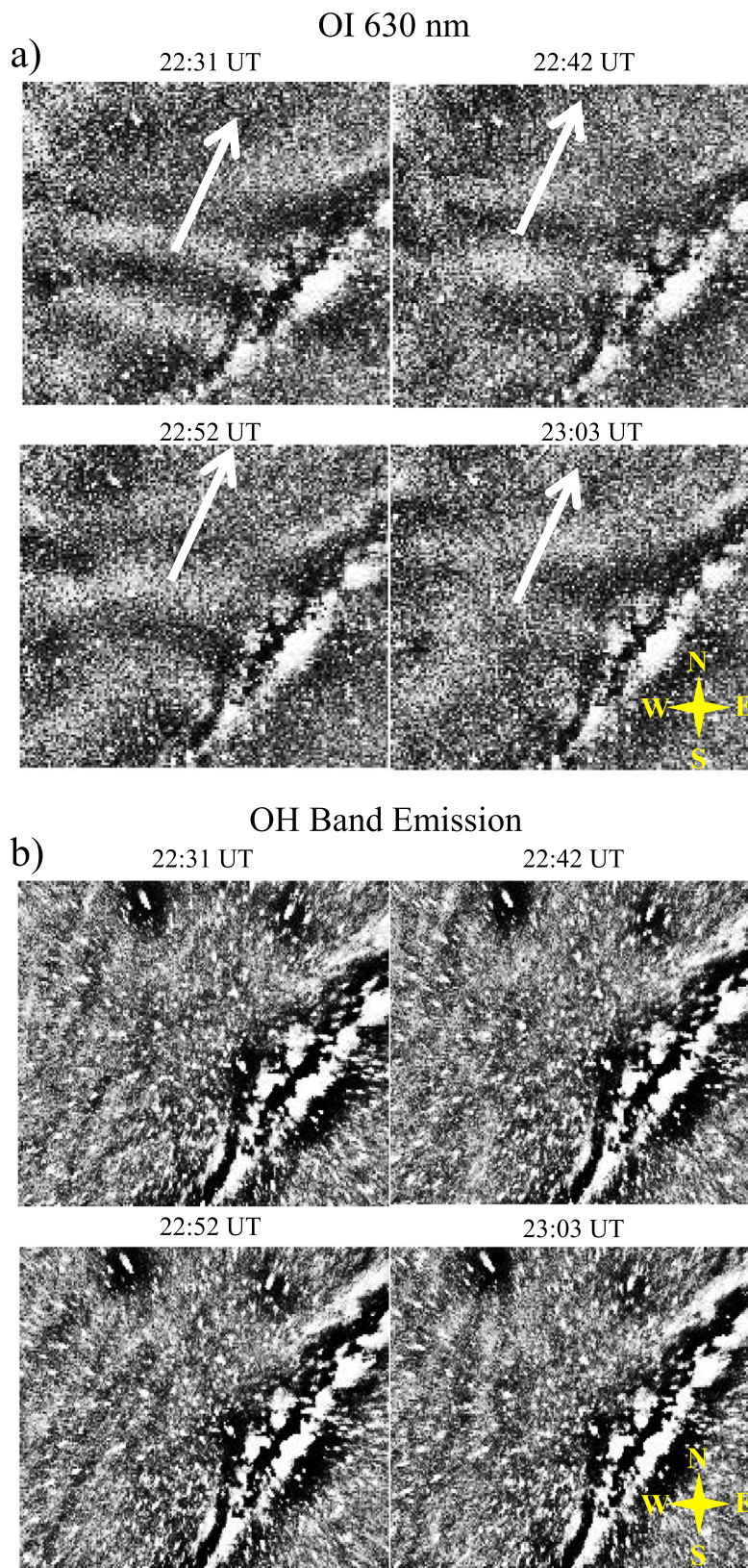
Figure 5. (a) A sequence of OI 630.0-nm unwarped images on the night of 2 August 2013, between 22:31 and 23:03 UT, at Cachoeira Paulista. The white arrows indicate periodic medium-scale traveling ionospheric disturbance propagating to the north-northeast. (b) OH unwarped images, in the same span of OI 630-nm images, with the goal to check if there is any contamination of OH emission in the OI 630-nm image.
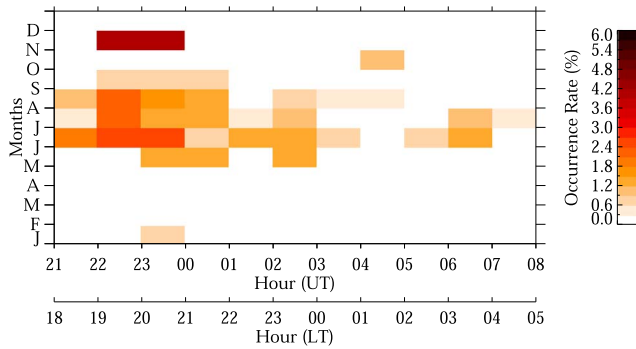
Figure 6. Monthly occurrence rate of periodic medium-scale traveling ionospheric disturbances versus time. The months are represented by the initials of their respective names.

observed through the Swarm satellite constellation, from November 2013 to March 2015. The authors associated the fluctuations in the magnetic field as being due to Perkins instability MSTIDs. They also observed that, in December, MSTIDs occurrence rate is very low in Brazilian south-southeast. On the other hand, in June, the occurrence rate of MSTIDs is high, our results corroborating them. Park et al. (2015) also show that during southern equinox there was no occurrence of MSTIDs. Observations of MSTIDs in the Japanese sector are more frequent during northern summer (Shiokawa, Ihara, et al., 2003). However, the occurrence of MSTIDs observed in Arecibo (18.3°N, 66.7°W) by Garcia et al. (2000) and Martinis et al. (2010) is also frequent in northern winter.

Observational and numerical studies showed that the polarization electric field in the E region plays a preponderant role in the formation of dark band MSTIDs by mapping the electric field along the magnetic field lines between E and F regions (Cosgrove, 2007; Otsuka et al., 2008; Saito et al., 2007; Yokoyama et al., 2009). Martinis et al. (2010) reported that the coupling mechanism between regions E and F is not sufficient to explain the results obtained. An explanation for the occurrence of MSTIDs in southern and northern winter months is presented by Shiokawa, Ihara, et al. (2003). The authors concluded that strong mesospheric winds are not capable of filtering the vertical propagation of gravity waves. Thus, the authors suggested that gravity waves, in the midlatitude MLT region, can propagate vertically and trigger the Perkins instability.
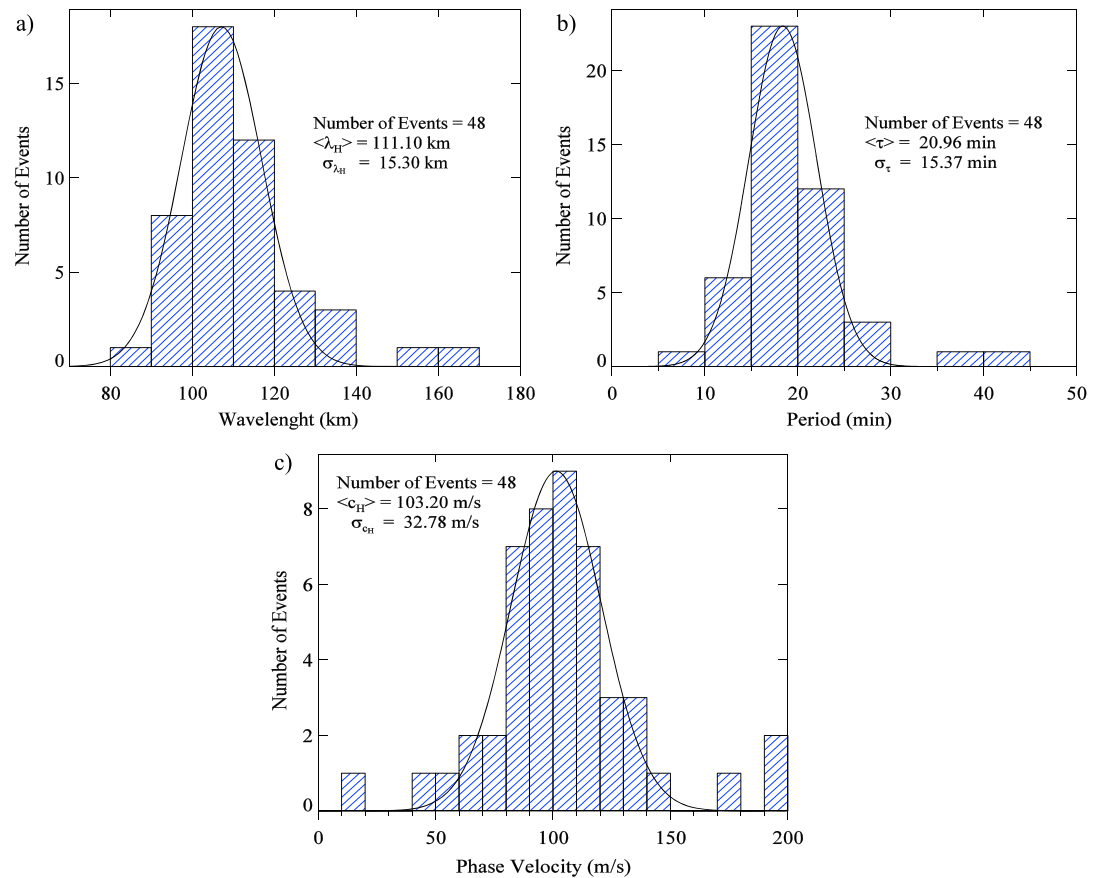
Figure 7. Distribution of wavelength (a), period (b), and phase velocity (c) of the periodic medium-scale traveling ionospheric disturbances observed at Cachoeira Paulista between June 2013 and December 2015. The continuous black line is a Gaussian fit to the data.
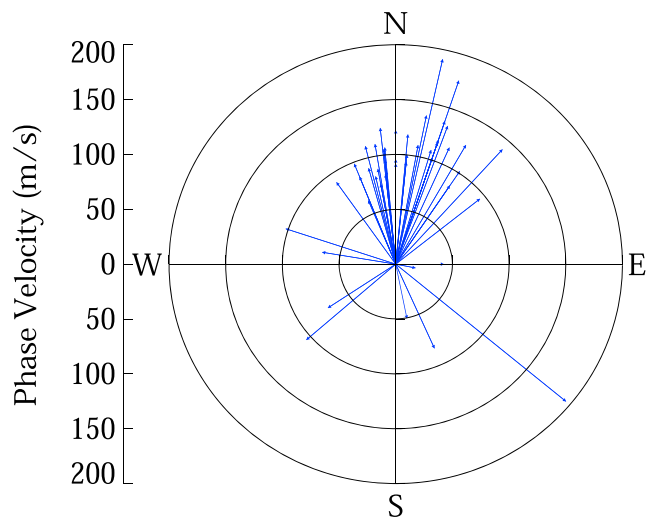
Figure 8. Propagation direction as a function of the horizontal phase velocity of the periodic medium-scale traveling ionospheric disturbances observed between June 2013 and December 2015.

Another point to be considered is that MSTIDs may have an interhemispheric coupling through the magnetic flux tube at conjugated points. Shiokawa, Otsuka, et al. (2003) and Otsuka et al. (2004) showed MSTIDs associated with fluctuations in the electric field; therefore, they tend to occur simultaneously in both hemispheres. Similar results were found by Stefanello et al. (2015) in the south of Brazil.

Furthermore, MSTIDs are originated in midlatitudes and not all of them can reach Brazilian south-southeast. The preferential propagation direction of MSTIDs, northwestward, makes them travel long distances without energy dissipation (Kelley, 2011). Narayanan et al. (2014) analyzed 2 years of data obtained from OI 630.0-nm emission in Yonaguni (24.5°N, 123.0°L), Japan. The authors observed that MSTIDs rarely propagate to magnetic latitudes less than 15°, and it occurs during the low solar activity period. Narayanan et al. (2014) pointed out two physical explanations for that: first, the increasing intensity due to midnight pressure bulge shift to the poles (further details about midnight pressure bulge can be found in Figueiredo, Buriti, et al., 2017; Mesquita et al., 2018) when MSTIDs occur late at night and second, when MSTIDs propagate before midnight, it encounters the equatorial ionization anomaly that limits its propagation toward the equator.

Regarding the influence of solar activity on the observation of dark band MSTIDs, Candido et al. (2008) and Amorim et al. (2011) observed around 10 years of data from OI 630.0-nm images. Candido et al. (2008) and Amorim et al. (2011) suggested that Perkins instability does not develop during high solar activity due to the frequency of ion-neutral collision being inversely proportional to the growth rate of Perkins instability, which corroborates the little observation of dark band MSTIDs in the present study.

Concerning about MSTIDs propagation direction and phase velocity, the present study's results are consistent when compared to the results obtained by Amorim et al. (2011), Candido et al. (2008), and Pimenta, Amorim, and Candido (2008), which presented velocities ranging from 50 to 100 m/s. The MSTIDs show propagation direction to northwest in the Southern Hemisphere; the mechanism of generation and preferential direction are due to Perkins instability (Amorim et al., 2011; Duly et al., 2013; Martinis et al., 2010) and the electrodynamics coupling between the regions *E* and *F* (Cosgrove & Tsunoda, 2004; Cosgrove et al., 2004; Haldoupis et al., 1996; Kelley et al., 2003; Otsuka et al., 2007; Tsunoda, 1998; Tsunoda & Cosgrove, 2001; Yokoyama & Hysell, 2010; Yokoyama et al., 2009, 2004), respectively. Therefore, the results observed in the present work corroborate the results obtained by Duly et al. (2013), Martinis et al. (2010), and Amorim et al. (2011).

4.2. Periodic MSTIDs

The seasonality of occurrence is the same for periodic and dark band MSTIDs, that is, during southern winter and southern spring months; the only notable difference is in the time of occurrence. It can be seen that periodic MSTIDs occur earlier than dark band MSTIDs. Our results corroborate the results of Paulino et al. (2016), who observed a higher occurrence of periodic MSTIDs between May and September, and Shiokawa et al. (2006) and Fukushima et al. (2012), who observed that the occurrence of MSTIDs is higher between May

Table 1
Characteristics of the Two Types of Nighttime MSTIDs Observed in Literature

Characteristic	Perkins MSTIDs	Gravity waves MSTIDs
Observation occurrence	Summer (midlatitudes) winter and equinox (low latitudes)	Winter and equinox (low latitudes)
Propagation direction	Northwest and (southwest) in Southern and (Northern) Hemispheres	All directions
Horizontal wavelength	100–450 km	80–700 km
Period	10–60 min	10–60 min
Horizontal phase velocity	20–200 m/s	40–350 m/s

Note. MSTIDs = medium-scale traveling ionospheric disturbances.

and July–October in Indonesia. In southern summer, it is not possible to verify the occurrence of dark band and periodic MSTIDs due to cloud cover.

Regarding the observed wave parameters, Paulino et al. (2016) pointed out that MSTIDs do not have a horizontal wavelength greater than 200 km and less than 80 km with mean horizontal wavelengths of 145 ± 25 km. The present study's results were similar to them. However, Fukushima et al. (2012) found MSTIDs with a mean horizontal wavelength of 790 ± 440 km, which is much higher than those observed in Brazil. Paulino et al. (2016) showed that periodic MSTIDs present a mean observed period of 22 ± 11 min, and our present results corroborate theirs. In Indonesia, Fukushima et al. (2012) observed that MSTIDs had period between 40 and 50 min with mean value and standard deviation of 42 ± 11 min. The horizontal phase velocities of the present study are similar to those presented by Paulino et al. (2016). However, comparing the horizontal phase velocities of the present study with those presented by Fukushima et al. (2012), the horizontal phase velocities obtained in Indonesia are 3 times higher than ours. Paulino et al. (2018) observed that the intrinsic period of periodic MSTIDs is smaller than the observed period resulting in higher phase velocity. In India, Sau et al. (2018) observed periodic MSTIDs with the period, phase velocities, and wavelength in the range of 25–75 min, 70–160 m/s, and 130–575 km, respectively. The authors observed propagation direction of periodic MSTIDs, during the equinox, propagating toward north-northwest, while during the winter there was no specific propagation direction. The period and phase velocities reported in our present study are comparable to the values reported by Sau et al. (2018). On the other hand, the propagation direction and wavelength are different. We also compared the present results with the gravity wave characteristic observed in upper mesosphere and lower thermosphere (MLT) regions. Comparing to the results reported by Wrasse et al. (2006) and Medeiros et al. (2004), we found that periodic MSTIDs are much faster than gravity waves in MLT heights, where these waves have phase velocities between 10 and 70 m/s. For gravity waves that propagate directly from the troposphere to the thermosphere, it is necessary to have phase speeds greater than 100 m/s, because they are less susceptible to dissipative processes such as kinetic molecular viscosity, which is the main mechanism of filtering in thermosphere (Vadas, 2007).

The propagation directions of the present work are distinct from the results previously observed. Shiokawa et al. (2006) and Fukushima et al. (2012) verified that most waves propagate to south and southwest. On the other hand, Paulino et al. (2016, 2018) observed that MSTIDs propagation direction is to northwest, north, northeast, and southeast. These comparisons suggest that the sources of periodic MSTIDs observed in the current study and Paulino et al. (2016, 2018) are similar, but the location of the source is different. Another explanation for these differences in MSTIDs propagation direction may be related to wind filtering process (e.g., American sector: Paulino et al., 2018, and Asian sector: Medvedev et al., 2017) and location of the sources (e.g., American sector: Figueiredo et al., 2018 and Asian sector: Fukushima et al., 2012) which, a priori, are different between the American and Asian sectors. Furthermore, Miyoshi et al. (2014) show that longitudinal variability of upward gravity waves energy can affect the longitudinal variability in the ionosphere.

The propagation direction of periodic MSTIDs may have three reasons: first, MSTIDs have been thought to be caused by atmospheric gravity waves (Hines, 1960; Hooke, 1968), because MSTIDs are observed to propagate equatorward, one is the changing gravity wave source region for the observer and the other might be an effect of wave filtering by background wind in the thermosphere.

The gravity wave is an oscillation of neutral particles. Through ion-neutral collisions, ions in the F region move along the geomagnetic field lines. Hooke (1968) has shown that the velocity of the ion motion along the geomagnetic field is the same as that of neutral motion along the geomagnetic field caused by gravity waves. Ion motion across the magnetic field line (**B**) is restricted because the ion gyrofrequency is much higher than the ion-neutral collision frequency. This directivity of the ion mobility causes directivity in the response of the electron density variations to the neutral motion caused by gravity waves. Since neutral particle oscillation parallel to **B** is larger for gravity waves propagating equatorward than for those propagating to other directions, equatorward propagating gravity waves could cause a larger amplitude of plasma density perturbations than gravity waves propagating in other directions (Hooke, 1970). Such directivity in response to the F region plasma of gravity waves could be responsible for the equatorward preference in MSTID propagation direction. However, the magnetic equator, in the South American continent, has a very pronounced declination (between 15° and 20° W in south-southeast of Brazil, declination calculated for 2015). If we assume this hypothesis as the main mechanism to explain the propagation direction, periodic MSTIDs should propagate

only toward the magnetic field lines (observed only ~21%). Most periodic MSTIDs show direction of propagation to the north-northeast (~60%), suggesting that another mechanism should be responsible for the direction of propagation of periodic MSTIDs.

Figueiredo et al. (2018) observed that daytime MSTIDs propagation direction in southern winter months is to north and northeast, over the South American continent. The authors showed a good correlation between daytime MSTID propagation direction and the location of the southern winter convective storms associated with cold front and jet stream in the Brazilian South. They suggested that daytime MSTIDs propagation direction may be associated with the location of the sources in the troposphere. Most of periodic MSTIDs propagate to north and northeast in southern winter months. Then, we suggest that a possible explanation of the propagation direction of MSTIDs might be due to the location of the source of upward gravity waves.

Wrasse et al. (2006) and Medeiros et al. (2004) observed MLT gravity waves propagating to west-northwest during southern winter, whereas most of the periodic MSTIDs propagation directions are to north and northeast. Medeiros et al. (2004) made a study to verify the process of neutral wind filtering of gravity wave in MLT region, and the current work will follow the same procedure for thermosphere.

4.2.1. Wind Filtering of Periodic MSTIDs

The wind filtering process occurs when the wind speed is equal to the periodic MSTID velocity. When this occurs, it is called critical level (Vadas, 2007). From the definition of critical level, one can construct horizontal surfaces by polar graphs, commonly called wind blocking diagram, in which we see the velocities and angles where the gravity waves cannot propagate vertically due to the neutral wind filtering process. The critical level values that are being discussed are below 120 m/s; similar values were observed by Paulino et al. (2018). Periodic MSTIDs with horizontal phase velocity and propagation direction within these regions are absorbed (Campos et al., 2016; Medeiros et al., 2003, references therein).

The intrinsic frequency of gravity waves ($\widehat{\omega}$), under the influence of horizontal neutral wind, is described by Gossard and Hooke (1975, page 122):

$$\widehat{\omega} = \overrightarrow{k} \cdot \left(\overrightarrow{c} - \overrightarrow{v} \right), \tag{1}$$

in which $\overrightarrow{k}$ is the horizontal wave vector, $\overrightarrow{c}$ is the phase velocity of the wave, and $\overrightarrow{v}$ is the neutral wind speed as a function of altitude. When the wave moves faster than wind, $\widehat{\omega}$ is positive, and when the reverse occurs, it is negative. Defining $\overrightarrow{c} = \omega / \overrightarrow{k}$, in which ω is the observed frequency, we can rewrite equation (1) as follows:

$$\widehat{\omega} = \omega \left(1 - \frac{\overrightarrow{v}}{\overrightarrow{c}} \right). \tag{2}$$

Rewriting equation (2) according to the zonal and meridional components of neutral wind (v_z, v_m), we get the following:

$$\widehat{\omega} = \omega \left(1 - \frac{v_z \cos(\phi) + v_m \sin(\phi)}{\overrightarrow{c}} \right). \tag{3}$$

In this way, when gravity waves reach some critical level, the neutral wind is equal to the phase velocity of the wave ($\overrightarrow{v} = \overrightarrow{c}$); then $\widehat{\omega} \rightarrow 0$, and the wave is absorbed. The forbidden regions (block diagram) at any height below the peak of the emission layer and for each propagation direction (ϕ) and $\overrightarrow{c}$. Therefore, the block diagram in polar ($\overrightarrow{c}$ as the radius and ϕ as the polar angle) form is defined by the following:

$$\overrightarrow{c} = v_z \cos(\phi) + v_m \sin(\phi). \tag{4}$$

The neutral wind model used to construct the block diagrams is Horizontal Wind Model-2007; further details can be found at Drob et al. (2008). In this work, the block diagram was calculated from the surface up to 300 km of altitude, step of 1 km, for the geographic coordinates at Cachoeira Paulista. We also used the parameters for moderate solar activity, 120 SFU (1 SFU = 10^{-22} Wm^{-2} Hz^{-1}), for 24:00 UT, and quiet magnetic activity ($Kp \leq 4$).
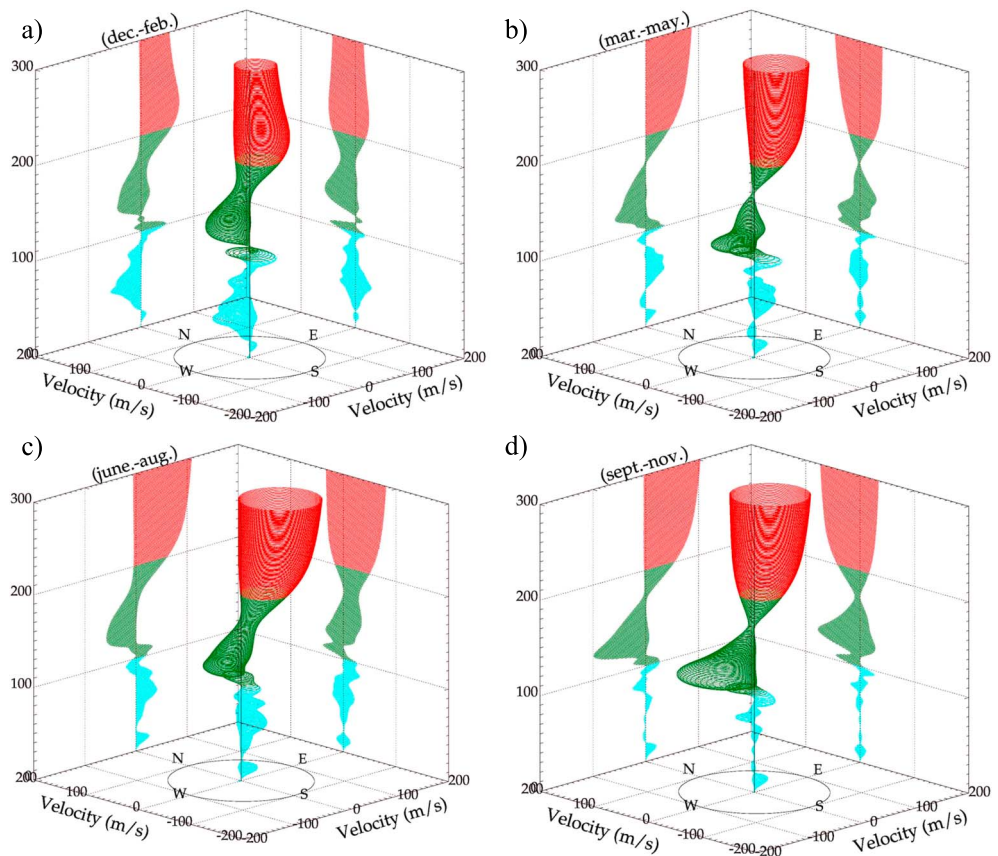
Figure 9. Wind blocking diagram for neutral wind. Circles represent regions where periodic medium-scale traveling ionospheric disturbances would be absorbed by the basic wind, and in these conditions wave would not propagate vertically. Seasons are arranged as follows: (a) southern summer, (b) southern autumn, (c) southern winter, and (d) southern spring. The height interval of each circle is 1 km.

Figure 9 shows the blocking diagrams for southern summer (an average of all days between December and February), southern autumn (an average of all days between March and May), southern winter (an average of all days between June and August), and southern spring (an average of all days between September and November) for 2013. To facilitate the understanding of the graphic, winds were separated into three height intervals with distinct colors: cyan (0–99 km), green (100–199 km), and red (200–300 km). The black circle at the bottom of Figure 9 informs the geographical directions, while the axes indicate the magnitude of the wind. It is observed in Figure 9 to the seasonal variation of the winds during southern summer and southern winter solstices in MLT and thermosphere/ionosphere regions. According to Medeiros et al. (2003), MLT neutral winds play a role in gravity wave filtering at Cachoeira Paulista for the gravity waves observed in the mesosphere region.

Figure 10 shows two-dimensional wind blocking diagram with propagation directions of periodic MSTIDs (blue arrows) for each southern season. The colors for each height range are the same as shown in Figure 9. It can be noticed that most of periodic MSTIDs have not been wind filtered. Wrasse et al. (2006) and Medeiros et al. (2004) concluded that the background wind is an important filtering process of gravity waves in the MLT region. However, periodic MSTIDs are faster than gravity waves observed in MLT and do not suffer the influence of background wind. Paulino et al. (2018) observed that propagation direction of periodic MSTIDs can be satisfactorily explained by the influence of background wind above the MLT region. It is interesting that most periodic MSTIDs have propagation direction opposite to the background wind direction as shown by Paulino et al. (2018); this evidence shows us that the background wind also has a significant importance in the propagation direction of periodic MSTIDs, and it has shown that gravity waves resulting in MSTID can propagate from the troposphere to the thermosphere without reaching the critical level.
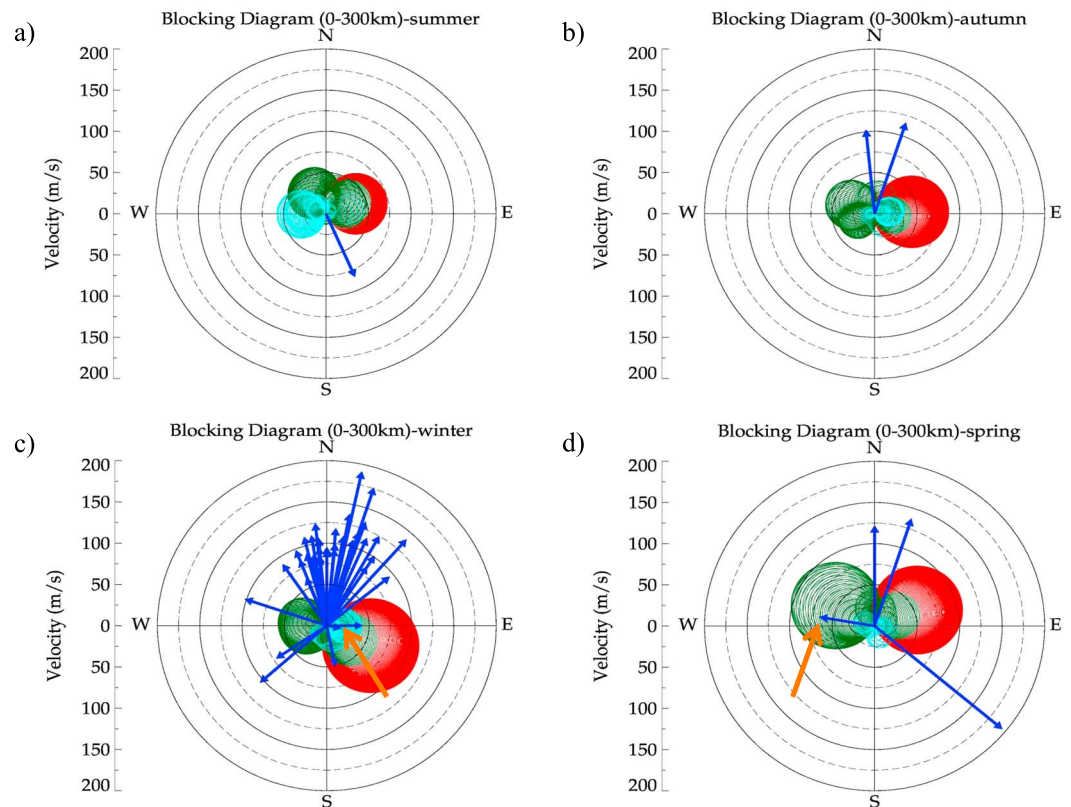
Figure 10. Two-dimensional wind blocking diagram for each season, (a) southern summer, (b) southern autumn, (c) southern winter, and (d) southern spring, in which colored circles are regions where there is no wave propagation due to the effect of critical levels. The altitude ranges were separated by colors: cyan (0–99 km), green (100–199 km), and red (200–300 km). The propagation directions of periodic medium-scale traveling ionospheric disturbances are indicated by blue arrows, and orange arrows indicate periodic medium-scale traveling ionospheric disturbances that are within the blocking region.

It is observed in Figure 10 that three cases of waves are within the blocking region, indicated by orange arrows. Using the model results of Vadas (2007) and comparing with the mean parameters of periodic MSTIDs ($\lambda_H = 111 \pm 15$ km, $\tau = 21 \pm 15$ min, and $C_H = 103 \pm 33$ m/s). We observed that gravity waves from troposphere dissipate above 150 km. It might be that secondary waves are generated from the momentum and energy deposition of gravity waves of the lower atmosphere and disturb the OI 630.0-nm layer (e.g., Vadas & Nicolls, 2009). In order to further investigate it, however, it is necessary to have a better idea whether the observed MSTIDs were originated from the troposphere or from any other wave sources. The Vadas (2007) ray tracing method would be helpful to understand in which region of the atmosphere MSTIDs are originated. The method shows, in a realistic model, dissipation properties such as periods, dissipation altitude, horizontal phase velocities, and horizontal distance traveled for gravity waves launched at different altitudes as functions of horizontal and vertical wavelengths. Furthermore, Vadas (2007) shows, in a didactic way, how to interpret the results when we compare it with the parameters of observed MSTIDs.

5. Conclusion

In this paper, about 2.5 years of thermospheric OI 630.0-nm image data were used to observe nighttime MSTIDs with the goal of study their morphology and characteristics in the Brazilian South-Southeast. The main results and conclusions obtained in this work were the following:

Two distinct types of nighttime MSTIDs have been identified and classified in relation to their morphology and wave characteristics: dark bands have a well-defined wavefront followed by a decrease in airglow intensity with propagation direction mechanism associated with electrodynamics coupling between the E and F regions. Dark band MSTIDs structures caused by Perkins instability are interlinked with the sporadic E layer

instability. On the other hand, periodic MSTIDs have wave train and may be associated with the propagation of gravity waves. Because of these differences in waveform morphology and parameters, we suggest to the scientific community to have different terminologies for nighttime MSTIDs: those that are generated by Perkins instability and have electrodynamics characteristics are called Perkins MSTIDs, and the MSTIDs that have gravity waves characteristics are called gravity waves MSTIDs.

The monthly occurrence of nighttime MSTIDs is between April and November. The time occurrence of dark band MSTIDs is after 01:00 UT (22:00 LT), while the time occurrence of the periodic MSTIDs is between 21:00 (18:00 LT) and 03:00 UT (24:00 LT).

The average horizontal phase velocity of dark band MSTIDs is 115.64 ± 34.48 m/s. Periodic MSTIDs present horizontal wavelength, period, and average horizontal phase velocity of 144.8 ± 24.8 km, 20.96 ± 15.37 min, and 103.20 ± 32.78 m/s, respectively.

The propagation direction of nighttime MSTIDs showed to be anisotropic. Dark band MSTIDs propagate to northwestward, which is explained by the well-known Perkins instability theory. On the other hand, periodic MSTIDs propagate mainly to north-northeastward. To explain the periodic MSTIDs propagation direction, three hypotheses are suggested: neutral wind filtering process, neutral motion along geomagnetic field caused by gravity waves, and the location of the source. We realize that the three combined hypotheses may be the mechanism that controls periodic MSTIDs propagation direction.

In this study, we have shown that gravity waves resulting in periodic MSTIDs can propagate from the troposphere to the thermosphere without reaching the critical level.

References

Alimov, V. A., Vybornov, F. I., & Rakhlin, A. V. (2008). On the fractal structure of small-scale traveling ionospheric disturbances. *Radiophysics and Quantum Electronics*, *51*, 20–27. https://doi.org/10.1007/s11141-008-9001-2

Amorim, D. C. M., Pimenta, A. A., Bittencourt, J. A., & Fagundes, P. R. (2011). Long term study of medium-scale traveling ionospheric disturbances using oi 630 nm all sky imaging and ionosonde over Brazilian low latitudes. *Journal of Geophysical Research*, *116*, A06312. https://doi.org/10.1029/2010JA016090

Bageston, J. V., Wrasse, C. M., Batista, P. P., Hibbins, R. E., Fritts, D. C., Gobbi, D., & Andrioli, V. F. (2011). Observation of a mesospheric front in a thermal-doppler duct over King George Island, Antarctica. *Atmospheric Chemistry and Physics*, *23*(11), 12,137–12,147. https://doi.org/10.5194/acp-11-12137-2011

Behnke, R. (1979). *F* layer height bands in the nocturnal ionosphere over Arecibo. *Journal of Geophysical Research*, *84*, 974–978. https://doi.org/10.1029/JA084iA03p00974

Bowman, G. G. (1985). Some aspects of mid-latitude spread-Es and its relationship with spread-F. *Planetary and Space Science*, *33*(9), 1081–1089. https://doi.org/10.1016/0032-0633(85)90027-3

Bowman, G. G. (1989). Quasi-periodic scintillations at mid-latitudes and their possible association with ionospheric sporadic-E structures. *Annales de Geophysique*, *7*, 259–267.

Campos, J. A. V., Paulino, I., Wrasse, C. M., Medeiros, A. F., Paulino, A. R., & Buriti, R. A. (2016). Observations of small-scale gravity waves in the equatorial upper mesosphere. *Revista Brasileira de Geofísica*, *34*(4), 10. https://doi.org/10.22564/rbgf.v34i4.876

Candido, C. M. N., Pimenta, A. A., Bittencourt, J. A., & Becker-Guedes, F. (2008). Statistical analysis of the occurrence of medium-scale traveling ionospheric disturbances over Brazilian low latitudes using OI 630.0 nm emission all-sky images. *Journal of Geophysical Research*, *35*, L17105. https://doi.org/10.1029/2008GL035043

Cosgrove, R. B. (2007). Generation of mesoscale F layer structure and electric fields by the combined Perkins and Es layer instabilities, in simulations. *Annales Geophysicae*, *25*, 1579–1601. https://doi.org/10.5194/angeo-25-1579-2007

Cosgrove, R. B., & Tsunoda, R. T. (2003). Simulation of the nonlinear evolution of the sporadic-*E* layer instability in the nighttime midlatitude ionosphere. *Journal of Geophysical Research*, *108*(A7), 1283. https://doi.org/10.1029/2002JA009728

Cosgrove, R. B., & Tsunoda, R. T. (2004). Instability of the E-F coupled nighttime midlatitude ionosphere. *Journal of Geophysical Research*, *109*, A04305. https://doi.org/10.1029/2003JA010243

Cosgrove, R. B., Tsunoda, R. T., Fukao, S., & Yamamoto, M. (2004). Coupling of the Perkins instability and the sporadic E layer instability derived from physical arguments. *Journal of Geophysical Research*, *109*, A06301. https://doi.org/10.1029/2003JA010295

Drob, D., Emmert, J., Crowley, G., Picone, J., Shepherd, G., Skinner, W., et al. (2008). An empirical model of the Earth's horizontal wind fields: HWM07. *Journal of Geophysical Research*, *113*, A12304. https://doi.org/10.1029/2008JA013668

Duly, T. M., Chapagain, N. P., & Makela, J. J. (2013). Climatology of nighttime medium-scale traveling ionospheric disturbances (MSTIDS) in the Central Pacific and South American sectors. *Annales Geophysicae*, *31*(12), 2229–2237. https://doi.org/10.5194/angeo-31-2229-2013

Figueiredo, C. A. O. B., Buriti, R. A., Paulino, I., Meriwether, J. W., Makela, J. J., Batista, I. S., et al. (2017). Effects of the midnight temperature maximum observed in the thermosphere–ionosphere over the northeast of Brazil. *Annales de Geophysique*, *35*, 953–963. https://doi.org/10.5194/angeo-35-953-2017

Figueiredo, C. A. O. B., Takahashi, H., Wrasse, C. M., Otsuka, Y., Shiokawa, K., & Barros, D. (2018). Medium-scale traveling ionospheric disturbances observed by detrended total electron content maps over Brazil. *Journal of Geophysical Research: Space Physics*, *123*, 2215–2227. https://doi.org/10.1002/2017JA025021

Figueiredo, C. A. O. B., Wrasse, C. M., Takahashi, H., Otsuka, Y., Shiokawa, K., & Barros, D. (2017). Large-scale traveling ionospheric disturbances observed by GPS dTEC maps over North and South America on Saint Patrick's Day storm in 2015. *Journal of Geophysical Research: Space Physics*, *122*, 4755–4763. https://doi.org/10.1002/2016JA023417

Forbes, J. M., Bruinsma, S. L., Doornbos, E., & Zhang, X. (2016). Gravity wave-induced variability of the middle thermosphere. *Journal of Geophysical Research: Space Physics*, *121*, 6914–6923. https://doi.org/10.1002/2016JA022923

Francis, S. H. (1974). A theory of medium-scale traveling ionospheric disturbances. *Journal of Geophysical Research*, *79*, 5245–5260. https://doi.org/10.1029/JA079i034p05245

Fukao, S., Kelley, M. C., Shirakawa, T., Takami, T., Yamamoto, M., Tsuda, T., & Kato, S. (1991). Turbulent upwelling of the mid-latitude ionosphere: 1. Observational results by the mu radar. *Journal of Geophysical Research*, *96*, 3725–3746. https://doi.org/10.1029/90JA02253

Fukushima, D., Shiokawa, K., Otsuka, Y., & Ogawa, T. (2012). Observation of equatorial nighttime medium-scale traveling ionospheric disturbances in 630-nm airglow images over 7 years. *Journal of Geophysical Research*, *117*, A10324. https://doi.org/10.1029/2012JA017758

Garcia, F. J., Kelley, M. C., Makela, J. J., & Huang, C.-S. (2000). Airglow observations of mesoscale low-velocity traveling ionospheric disturbances at midlatitudes. *Journal of Geophysical Research*, *105*, 407–18,415. https://doi.org/10.1029/1999JA000305

Gossard, E., & Hooke, W. (1975). *Waves in the atmosphere*. New York: Elsevier.

Haldoupis, C., Schlegel, K., & Farley, D. (1996). An explanation for type 1 radar echoes from the midlatitude *E*-region ionosphere. *Geophysical Research Letters*, *23*, 97–100. https://doi.org/10.1029/95GL03585

Hines, C. O. (1960). Internal atmospheric gravity waves at ionospheric heights. *Canadian Journal of Physics*, *38*(11), 1441–1481. https://doi.org/10.1139/p60-150

Hooke, W. H. (1968). Ionospheric irregularities produced by internal atmospheric gravity waves. *Journal of Atmospheric and Terrestrial Physics*, *30*(5), 795–823. https://doi.org/10.1016/S0021-9169(68)80033-9

Hooke, W. H. (1970). The ionospheric response to internal gravity waves 1. The *F* region response. *Journal of Geophysical Research*, *75*, 5535–5544. https://doi.org/10.1029/JA075i028p05535

Hunsucker, R. D. (1982). Atmospheric gravity waves generated in the high-latitude ionosphere: A review. *Reviews of Geophysics*, *20*, 293–315. https://doi.org/10.1029/RG020i002p00293

Kelley, M. C. (2011). On the origin of mesoscale TIDS at midlatitudes. *Annales Geophysicae*, *29*(2), 361–366. https://doi.org/10.5194/angeo-29-361-2011

Kelley, M. C., & Fukao, S. (1991). Turbulent upwelling of the mid-latitude ionosphere: 2. Theoretical framework. *Journal of Geophysical Research*, *96*, 3747–3753. https://doi.org/10.1029/90JA02252

Kelley, M. C., Haldoupis, C., Nicolls, M. J., Makela, J. J., Belehaki, A., Shalimov, S., & Wong, V. K. (2003). Case studies of coupling between the *E* and *F* regions during unstable sporadic-*E* conditions. *Journal of Geophysical Research*, *108*(A12), 1447. https://doi.org/10.1029/2003JA009955

Kelley, M. C., Makela, J. J., Saito, A., Aponte, N., Sulzer, M., & Gonzalez, S. A. (2000). On the electrical structure of airglow depletion/height layer bands over Arecibo. *Geophysical Research Letters*, *27*, 2837–2840. https://doi.org/10.1029/2000GL000024

Kotake, N., Otsuka, Y., Tsugawa, T., Ogawa, T., & Saito, A. (2006). Climatological study of GPS total electron content variations caused by medium-scale traveling ionospheric disturbances. *Journal of Geophysical Research*, *111*, A04306. https://doi.org/10.1029/2005JA011418

Makela, J. J., & Kelley, M. C. (2003). Using the 630.0-nm nightglow emission as a surrogate for the ionospheric Pedersen conductivity. *Journal of Geophysical Research*, *108*(A6), 1253. https://doi.org/10.1029/2003JA009894

Martinis, C., Baumgardner, J., Smith, S. M., Colerico, M., & Mendillo, M. (2006). Imaging science at El Leoncito, Argentina. *Annales Geophysicae*, *24*(5), 1375–1385. https://doi.org/10.5194/angeo-24-1375-2006

Martinis, C., Baumgardner, J., Wroten, J., & Mendillo, M. (2010). Seasonal dependence of MSTIDS obtained from 630.0 nm airglow imaging at Arecibo. *Geophysical Research Letters*, *37*, L11103. https://doi.org/10.1029/2010GL043569

Medeiros, A., Taylor, M. J., Takahashi, H., Batista, P., & Gobbi, D. (2003). An investigation of gravity wave activity in the low-latitude upper mesosphere: Propagation direction and wind filtering. *Journal of Geophysical Research*, *108*(D14), 4411. https://doi.org/10.1029/2002JD002593

Medeiros, A. F. D., Buriti, R., Machado, E., Takahashi, H., Batista, P. P., Gobbi, D., & Taylor, M. J. (2004). Comparison of gravity wave activity observed by airglow imaging at two different latitudes in Brazil. *Journal of Atmospheric and Solar - Terrestrial Physics*, *66*(6), 647–654.

Medvedev, A. V., Ratovsky, K. G., Tolstikov, M. V., Oinats, A. V., Alsatkin, S. S., & Zherebtsov, G. A. (2017). Relation of internal gravity wave anisotropy with neutral wind characteristics in the upper atmosphere. *Journal of Geophysical Research: Space Physics*, *122*, 7567–7580. https://doi.org/10.1002/2017JA024103

Mendillo, M., Baumgardner, J., Nottingham, D., Aarons, J., Reinisch, B., Scali, J., & Kelley, M. (1997). Investigations of thermospheric-ionospheric dynamics with 6300-Å images from the Arecibo Observatory. *Journal of Geophysical Research*, *102*, 7331–7343. https://doi.org/10.1029/96JA02786

Mesquita, R. L. A., Meriwether, J. W., Makela, J. J., Fisher, D. J., Harding, B. J., Sanders, S. C., et al. (2018). New results on the mid-latitude midnight temperature maximum. *Annales Geophysicae*, *36*, 541–553. https://doi.org/10.5194/angeo-36-541-2018

Miyoshi, Y., Fujiwara, H., Jin, H., & Shinagawa, H. (2014). A global view of gravity waves in the thermosphere simulated by a general circulation model. *Journal of Geophysical Research: Space Physics*, *119*, 5807–5820. https://doi.org/10.1002/2014JA019848

Munro, G. H. (1948). Short-period changes in the F region of the ionosphere. *Nature*, *162*(4127), 886–887. https://doi.org/10.1038/162886a0

Narayanan, V. L., Shiokawa, K., Otsuka, Y., & Saito, S. (2014). Airglow observations of nighttime medium-scale traveling ionospheric disturbances from Yonaguni: Statistical characteristics and low-latitude limit. *Journal of Geophysical Research: Space Physics*, *119*, 9268–9282. https://doi.org/10.1002/2014JA020368

Otsuka, Y., Onoma, F., Shiokawa, K., Ogawa, T., Yamamoto, M., & Fukao, S. (2007). Simultaneous observations of nighttime medium-scale traveling ionospheric disturbances and e region field-aligned irregularities at midlatitude. *Journal of Geophysical Research*, *112*, A06317. https://doi.org/10.1029/2005JA011548

Otsuka, Y., Shiokawa, K., Ogawa, T., & Wilkinson, P. (2004). Geomagnetic conjugate observations of medium-scale traveling ionospheric disturbances at midlatitude using all-sky airglow imagers. *Geophysical Research Letters*, *31*, L15803. https://doi.org/10.1029/2004GL020262

Otsuka, Y., Shiokawa, K., Ogawa, T., Yokoyama, T., & Yamamoto, M. (2009). Spatial relationship of nighttime medium-scale traveling ionospheric disturbances and *F* region field-aligned irregularities observed with two spaced all-sky airglow imagers and the middle and upper atmosphere radar. *Journal of Geophysical Research*, *114*, A05302. https://doi.org/10.1029/2008JA013902

Otsuka, Y., Suzuki, K., Nakagawa, S., Nishioka, M., Shiokawa, K., & Tsugawa, T. (2013). GPS observations of medium-scale traveling ionospheric disturbances over Europe. *Annales Geophysicae*, *31*(2), 163–172. https://doi.org/10.5194/angeo-31-163-2013

Otsuka, Y., Tani, T., Tsugawa, T., Ogawa, T., & Saito, A. (2008). Statistical study of relationship between medium-scale traveling ionospheric disturbance and sporadic *E* layer activities in summer night over Japan. *Journal of Atmospheric and Solar-Terrestrial Physics*, *70*(17), 2196–2202. https://doi.org/10.1016/j.jastp.2008.07.008

Park, J., Lühr, H., Kervalishvili, G., Rauberg, J., Michaelis, I., Stolle, C., & Kwak, Y.-S. (2015). Nighttime magnetic field fluctuations in the topside ionosphere at midlatitudes and their relation to medium-scale traveling ionospheric disturbances: The spatial structure and scale sizes. *Journal of Geophysical Research: Space Physics*, *120*, 6818–6830. https://doi.org/10.1002/2015JA021315

Paulino, I., Maranhão, G. L., Wrasse, C. M., Buriti, R. A., Medeiros, A. F., Paulino, A. R., et al. (2018). Intrinsic parameters of periodic waves observed in the OI 6300 airglow layer over the Brazilian equatorial region. *Annales Geophysicae*, *36*(1), 265–273, https://doi.org/10.5194/angeo-36-265-2018.

Paulino, I., Moraes, J. F., Medeiros, A. F., Vadas, S. L., Wrasse, C. M., Takahashi, H., et al. (2016). Periodic waves in the lower thermosphere observed by OI 630 nm airglow images. *Annales Geophysicae*, *34*(2), 293–301. https://doi.org/10.5194/angeo-34-293-2016

Pimenta, A. A., Amorim, D. C. M., & Candido, C. M. N. (2008). Thermospheric dark band structures at low latitudes in the Southern Hemisphere under different solar activity conditions: A study using OI 630 nm emission all-sky images. *Geophysical Research Letters*, *35*, L16103. https://doi.org/10.1029/2008GL034904

Pimenta, A. A., Kelley, M. C., Sahai, Y., Bittencourt, J. A., & Fagundes, P. R. (2008). Thermospheric dark band structures observed in all-sky OI 630 nm emission images over the Brazilian low-latitude sector. *Journal of Geophysical Research*, *113*, A01307. https://doi.org/10.1029/2007JA012444

Saito, S., Yamamoto, M., & Hashiguchi, H. (2008). Imaging observations of nighttime mid-latitude F-region field-aligned irregularities by an MU radar ultra-multi-channel system. *Annales Geophysicae*, *26*(8), 2345–2352.

Saito, S., Yamamoto, M., Hashiguchi, H., Maegawa, A., & Saito, A. (2007). Observational evidence of coupling between quasi-periodic echoes and medium scale traveling ionospheric disturbances. *Annales Geophysicae*, *25*(10), 2185–2194. https://doi.org/10.5194/angeo-25-2185-2007

Sau, S., Narayanan, V. L., Gurubaran, S., & Emperumal, K. (2018). Study of wave signatures observed in thermosphere airglow imaging over dip equatorial region. *Advanced space research*, *62*(7), 1762–1774. https://doi.org/10.1016/j.asr.2018.06.039

Shiokawa, K., Ihara, C., Otsuka, Y., & Ogawa, T. (2003). Statistical study of nighttime medium-scale traveling ionospheric disturbances using midlatitude airglow images. *Journal of Geophysical Research*, *108*(A1), 1052. https://doi.org/10.1029/2002JA009491

Shiokawa, K., Otsuka, Y., Ihara, C., Ogawa, T., & Rich, F. J. (2003). Ground and satellite observations of nighttime medium-scale traveling ionospheric disturbance at midlatitude. *Journal of Geophysical Research*, *108*(A4), 1145. https://doi.org/10.1029/2002JA009639

Shiokawa, K., Otsuka, Y., & Ogawa, T. (2006). Quasiperiodic southward moving waves in 630-nm airglow images in the equatorial thermosphere. *Journal of Geophysical Research*, *111*, A06301. https://doi.org/10.1029/2005JA011406

Shiokawa, K., Otsuka, Y., Tsugawa, T., Ogawa, T., Saito, A., Ohshima, K., et al. (2005). Geomagnetic conjugate observation of nighttime medium-scale and large-scale traveling ionospheric disturbances: FRONT3 campaign. *Journal of Geophysical Research*, *110*, A05303. https://doi.org/10.1029/2004JA010845

Sobral, J., Takahashi, H., Abdu, M., Taylor, M., Sawant, H., Santana, D. C., et al. (2001). Thermospheric F-region travelling disturbances detected at low latitude by an OI 630 nm digital imager system. *Advances in Space Research*, *27*, 1201–1206.

Stefanello, M., Muella, M., Amorim, D., Machado, C., Bageston, J., Pimenta, A., et al. (2015). OI 630.0 nm all-sky image observations of medium-scale traveling ionospheric disturbances at geomagnetic conjugate points. *Journal of Atmospheric and Solar-Terrestrial Physics*, *128*, 58–69. https://doi.org/10.1016/j.jastp.2015.03.012

Takahashi, H., Wrasse, C. M., Figueiredo, C. A. O. B., Barros, D., Abdu, M. A., Otsuka, Y., & Shiokawa, K. (2018). Equatorial plasma bubble seeding by MSTIDs in the ionosphere. *Progress in Earth and Planetary Science*, *5*(1), 32. https://doi.org/10.1186/s40645-018-0189-2

Tsunoda, R. T. (1998). On polarized frontal structures, type-1 and quasi-periodic echoes in midlatitude sporadic e. *Geophysical Research Letters*, *25*, 2641–2644. https://doi.org/10.1029/98GL01934

Tsunoda, R. T., & Cosgrove, R. B. (2001). Coupled electrodynamics in the nighttime midlatitude ionosphere. *Geophysical Research Letters*, *28*, 4171–4174. https://doi.org/10.1029/2001GL013245

Vadas, S. L. (2007). Horizontal and vertical propagation and dissipation of gravity waves in the thermosphere from lower atmospheric and thermospheric sources. *Journal of Geophysical Research*, *112*, A06305. https://doi.org/10.1029/2006JA011845

Vadas, S. L., & Nicolls, M. J. (2009). Temporal evolution of neutral, thermospheric winds and plasma response using PFISR measurements of gravity waves. *Journal of Atmospheric and Solar-Terrestrial Physics*, *71*(6-7), 744–770. https://doi.org/10.1016/j.jastp.2009.01.011

Wrasse, C., Nakamura, T., Tsuda, T., Takahashi, H., Medeiros, A., Taylor, M., et al. (2006). Reverse ray tracing of the mesospheric gravity waves observed at 23 s (Brazil) and 7 s (Indonesia) in airglow imagers. *Journal of Atmospheric and Solar-Terrestrial Physics*, *68*(2), 163–181. https://doi.org/10.1016/j.jastp.2005.10.012

Wrasse, C. M., Takahashi, H., Medeiros, A. F., Lima, L. M., Taylor, M. J., Gobbi, D., & Fechine, J. (2007). Determinação dos parâmetros de ondas de gravidade através da análise espectral de imagens de aeroluminescência. *Revista Brasileira de Geofísica*, *25*, 257–265. https://doi.org/10.1590/S0102-261X2007000300003

Yokoyama, T., Horinouchi, T., Yamamoto, M., & Fukao, S. (2004). Modulation of the midlatitude ionospheric E region by atmospheric gravity waves through polarization electric field. *Journal of Geophysical Research*, *109*, A12307. https://doi.org/10.1029/2004JA010508

Yokoyama, T., & Hysell, D. L. (2010). A new midlatitude ionosphere electrodynamics coupling model (MIECO): Latitudinal dependence and propagation of medium-scale traveling ionospheric disturbances. *Geophysical Research Letters*, *37*, L08105. https://doi.org/10.1029/2010GL042598

Yokoyama, T., Hysell, D. L., Otsuka, Y., & Yamamoto, M. (2009). Three-dimensional simulation of the coupled Perkins and Es-layer instabilities in the nighttime midlatitude ionosphere. *Journal of Geophysical Research*, *114*, A03308. https://doi.org/10.1029/2008JA013789